JOURNAL OF GEOPHYSICAL RESEARCH, VOL. 101, NO. C9, PAGES 20,669–20,686, SEPTEMBER 15, 1996

Remotely sensed surface currents in Monterey Bay from shore-based HF radar (Coastal Ocean Dynamics Application Radar)

Jeffrey D. Paduan and Leslie K. Rosenfeld[1]

Department of Oceanography, Naval Postgraduate School, Monterey, California

Abstract. Near-surface currents in Monterey Bay derived from a network of shore-based HF radars are presented for August–December 1994 and compared with those from April to September 1992. Focus is placed on the low-frequency (2- to 30-day period) motions in the remotely sensed data and on comparison of radar-derived currents with moored current and wind observations, ship-based acoustic Doppler current profiler observations, satellite-based surface temperature imagery, and surface drifter velocities. The radar-derived picture of the late summer mean flow is very similar in the two realizations and is consistent with historical data. Flow is equatorward in the outer part of the bay, poleward in a narrow band nearshore, and very sluggish in the middle of the bay. Low-pass-filtered time series of radar-derived currents are highly correlated with moored current observations and with winds in the outer part of the bay. The vector time series are also coherent across a broad frequency band with currents typically in phase between 1- and 9-m depths and with 1-m currents typically 40°–60° to the right of the wind. Overall, these results confirm the utility of Coastal Ocean Dynamics Applications Radar (CODAR)-type HF radars for the study of coastal surface currents out to ranges ~50 km from shore, particularly for highly averaged fields. Data variability and comparison with in situ observations for high-frequency (1- to 48-hour period) motions point to the need to better characterize and minimize sources of error in the radar observations.

1. Introduction

Currents near the ocean surface are critically important for many reasons, including influences on navigation, plankton ecology, and heat transports. Within the coastal zone these currents take on even more significance through their influences on recreation, search and rescue operations, hazardous material transport, and military strike capabilities and mine countermeasures. Making direct measurements of ocean currents is both difficult and expensive, particularly within the upper few meters of the water column due to the contaminating effects of surface waves and wind. In the coastal zone the destructive effect of accidental collisions with surface moorings is a real limitation. Even if these difficulties are overcome, it is impossible to obtain two-dimensional, continuous surface current observations using moored, ship-based, or drifting instruments. In this paper we report on near-surface current observations in the coastal waters around Monterey Bay, California. The measurements are both two-dimensional, with spatial resolution of a few kilometers, and continuous with temporal resolution of 2 hours. This is possible because the measurements derive from remotely sensed data from shore-based high-frequency (HF) radars.

As described below, the application of radar backscatter observations to ocean current measurements has taken place several times in recent decades, but there still exist many questions about the accuracy and stability of these techniques. In most cases the application of these techniques has been episodic and most deployments have been short term (order days or weeks) with minimal in situ measurements or calibration efforts. Exceptions include the multiple-year observations off Florida described by *McLeish and Maul* [1991] and the repeated deployments off the United Kingdom reviewed by *Prandle* [1991]. An important practical extension of these techniques, ship-based HF radar measurements, was implemented by *Teague* [1986] and recently attempted by *Gurgel* [1994] and by *Skop et al.* [1994]. We believe, however, that additional long-term, shore-based observations of the type described here are needed before operational uses of any HF radar system can begin.

We have three goals in the present study: (1) to show that the particular HF radar systems we have used provide useful and unique data when observations are low-pass filtered to remove random errors, (2) to describe the low-frequency, late summer surface circulation in and around Monterey Bay, and (3) to expose sources of errors in, and suggest possible improvements to, the real-time radar algorithms. This paper is organized as follows: the remainder of this section provides oceanographic and technical background, including the basic principles of HF radar techniques and existing knowledge about the circulation in and around Monterey Bay from conventional observations. Section 2 describes the remotely sensed and in situ data sets used in this study, including preliminary data collected with older-generation HF radar systems. Radar-derived versus in situ data comparisons are presented in section 3, and the low-frequency, two-dimensional radar-derived currents are presented in section 4. The final section summarizes the results of our 5-month-long current observations with particular emphasis on sources of error in

[1]Also at Monterey Bay Aquarium Research Institute, Moss Landing, California.

Paper number 96JC01663.

the radar data and suggestions for improving the radar-based techniques.

1.1. HF Radar Measurement of Surface Currents

Remotely sensed surface currents can be obtained by exploiting the backscattered signal from radars operating in the HF part of the electromagnetic spectrum (3–30 MHz). Wavelengths in the HF band are comparable to those of typical surface waves, which can lead to strong backscatter from the ocean surface. Resonant backscatter from the sea surface at these frequencies was first documented by *Crombie* [1955]. The link in this signal to near-surface currents was suggested by *Stewart and Joy* [1974]. Extensive reviews are given by *Fernandez* [1993] and *Prandle* [1991], but the basic principles are described here.

What makes the measurement possible is the fact that, within this frequency band, Bragg scattering from surface gravity waves, propagating radially with respect to the radar with exactly one half the wavelength of the incident energy, produces a very large spectral peak in the returned signal. The level of this peak is so much larger than the spectral levels due to reflection from other surfaces that it can be identified and its precise frequency determined. The Doppler frequency shift of the Bragg peak relative to the incident radar frequency is due to the velocity of the water plus the velocity of the reflecting surfaces, which are the gravity waves at one half the radar wavelength. In this case the motion of the reflecting surfaces is given by the phase speed of gravity waves in deep water: $c^2 = g\lambda/2\pi$, where g is the acceleration due to gravity and λ is the wavelength. Their contribution to the Doppler shift is therefore known. Any additional Doppler shift is attributed to the currents upon which the surface waves are riding. (For the radar wavelengths described below the deep water approximation is violated only in very shallow water of depths less than 6 m, which is not the case within our study area.)

Although backscattered energy from the Bragg scattering process is much greater than from other reflections, in practice, many observations must be averaged over a large area to obtain a statistically reliable estimate of the locations of the spectral peaks. Because of this, a single radar observation bin is of the order of 1–3 km wide and 1 hour in duration, and the resolution of the approaching or receding velocity is 4 cm s^{-1}. The offshore range of the measurements can be up to 60 km depending on propagation conditions and ocean wave heights. The depth extent of the measurements is a complicated function of the depth of influence of the surface waves responsible for the Bragg scattering. This is of the order of 1 m [*Stewart and Joy*, 1974], which is extremely close to the surface compared with more conventional current measurements.

A single HF radar installation can measure one velocity component of flow along radial lines emanating from the radar site. This is because the Bragg scattering is effective for waves traveling directly toward or away from the radar. In order to obtain a map of two-dimensional current flow over a large area, it is necessary to obtain measurements from at least two radars located in different places. Except for locations along the baseline between the radars, data from the two sites can be combined to estimate the vector currents. (Along the baseline, both instruments provide information about the same component of the currents, and neither instrument provides information about motions orthogonal to the baseline.) In general, these observations are not orthogonal. The error when producing vector current estimates is a function of the angle between the radial observations [*Prandle*, 1991; *Gurgel*, 1994]. Lower-resolution, higher-uncertainty mapping of vector currents has been attempted combining radial data from a single site at one time [*Fernandez*, 1993; *Shkedy et al.*, 1995] or from two sites at different times [*Prandle and Ryder*, 1985].

1.2. Phased Array Versus Direction Finding Antenna Systems

The measurement principle described above applies to any radar operated in the HF range. Various systems have been developed to exploit this principle, and they differ, mainly, in their antenna design. It is necessary to "point" the radar in different directions in order to observe the complete offshore sector. (Offshore distance can be determined by simple range gating of the signals.) The most straightforward pointing method at these frequencies is accomplished with a phased array of antennas spread over about 80 m of coastline. The time delay between elements of this line of antennas is used to sequentially point the radar in different directions. The Marconi company of the United Kingdom produces a commercial system called Ocean Surface Current Radar (OSCR) that employs the phased-array pointing method. Stanford University scientists also constructed a similar phased-array system. It was operated recently at Granite Canyon south of Monterey Bay [*Fernandez*, 1993] but tested originally north of Monterey Bay in the mid 1970s [*Ha*, 1979] and on board a research vessel during the Joint Air-Sea Interactions (JASIN) experiment [*Teague*, 1986].

Over 2 decades ago the National Oceanic and Atmospheric Administration's (NOAA) Wave Propagation Laboratory (WPL; now called Environmental Technologies Laboratory) began to develop a compact system using colocated antennas that can accomplish the necessary pointing without taking up large amounts of coastal real estate [*Barrick et al.*, 1977]. Such a system is also easier to transport and set up than phased-array systems. The instrument developed at WPL is called Coastal Ocean Dynamics Applications Radar (CODAR). The development and marketing of the CODAR-type HF radar system was taken over by Codar Ocean Sensors, Ltd. of the United States. Their second-generation instrument is called SeaSonde.

The CODAR pointing method employs direction-finding techniques, which are more complex than the beam-forming techniques used by phased-array systems. It relies on comparing the relative amplitudes of the returned energy on the various colocated antennas. CODAR systems have two crossed looped antennas mounted in orthogonal orientations with a single monopole antenna running through the center. Because each of these antenna elements has a different, and known, beam pattern as a function of look angle, the ratio of antenna signal strengths indicates directions from which the signals originated. A single composite spectrum, rather than a sequential set of spectra, is used to get information for all angles at a given range according to the method of *Lipa and Barrick* [1983]. Because of the additional limitations and error sources in direction-finding systems, and because of the more extensive set of published results based on the OSCR phased array system [e.g., *Prandle and Ryder*, 1985, 1989; *Prandle*, 1991; *Prandle et al.*, 1993; *Shay et al.*, 1995], testing, improvement, and use of the CODAR-type HF radar systems have been slow. Recently, *Masson* [1996] demonstrated the utility of CODAR data in her study of strong tidal currents off the British Columbia coast. We demonstrate here that the CODAR systems

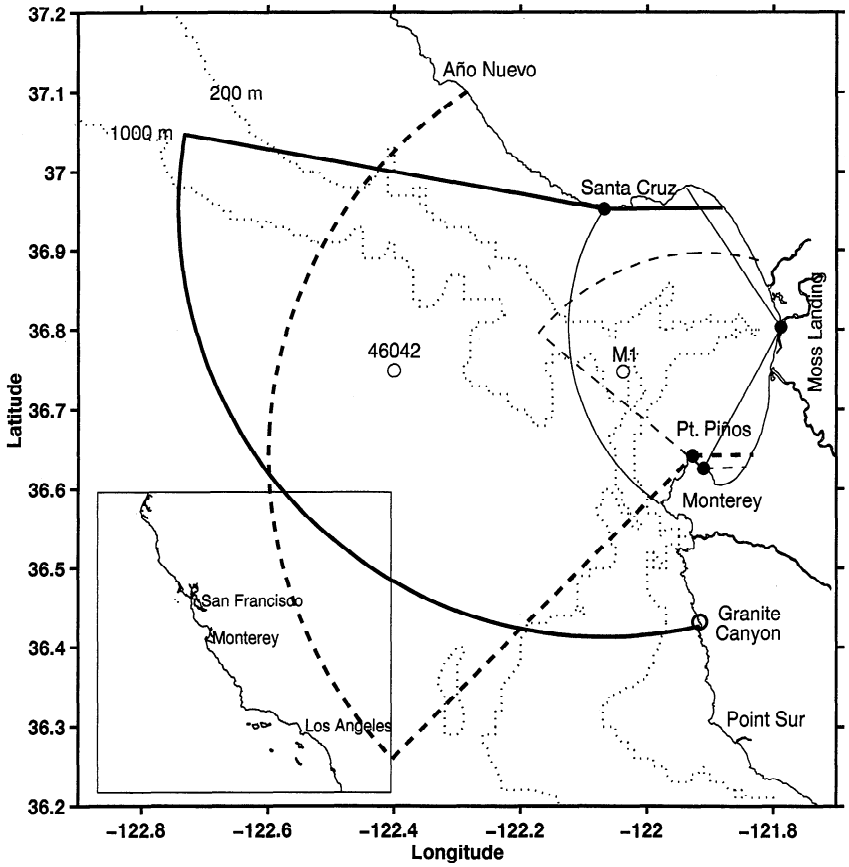

Figure 1. HF radar coverage areas around Monterey Bay used in this study. Arcs denote nominal range of radial current coverage for each site. Two-site data were collected in 1992 from CODARs in Moss Landing (thin solid line) and Monterey (thin dashed line). Three-site data were collected in 1994 from the CODAR in Moss Landing and SeaSondes in Santa Cruz (heavy solid line) and Point Pinos (heavy dashed line). SeaSonde data collected from Granite Canyon are not used in this study. Watch circles for moored current and wind (M1) and wind (46042) observations are also shown.

as they exist are also useful for low-frequency current observations. The small footprint and relatively low cost of CODAR-type systems suggest that they should be further developed in parallel with their phased-array counterparts.

1.3. Background on Monterey Bay Circulation

Monterey Bay is located 100 km south of San Francisco on the U.S. West Coast (Figure 1). There are few direct current measurements of any type available from the bay and, of course, none from so near the surface as those provided by CODAR. Recent studies of the circulation in the bay [*Rosenfeld et al.*, 1994a] have concentrated on the spring-summer period (March–July) when strong upwelling-favorable (i.e., equatorward alongshore component) winds result in the strongest near-surface temperature gradients and the greatest biological productivity. During periods of upwelling-favorable winds, which are prevalent during this time of year, there is a band of cold water which flows equatorward across the mouth of Monterey Bay with typical near-surface speeds of 20–30 cm s^{-1} [*Rosenfeld et al.*, 1994a, 1995]. Upwelling centers are located north and south of Monterey Bay near Point Año Nuevo and Point Sur, respectively. A warm anticyclonic feature is often found off Monterey Bay, or just to the south of it [*Rosenfeld et al.*, 1994a; S. R. Ramp et al., Moored observations of the current and temperature structure over the continental slope off central California, 1, A basic description of the variability, submitted to *Journal of Geophysical Research*, 1996; hereinafter referred to as Ramp et al., submitted manuscript, 1996]. This feature was also seen in advanced very high resolution radiometer (AVHRR) imagery and conductivity-temperature-depth (CTD) data in November 1988 [*Tisch et al.*, 1992].

Less attention has been paid to the late summer and fall, which is a time of transition from the upwelling regime to the winter storm-dominated situation. Here we review what is known of the late summer near-surface flow in this region. *Skogsberg* [1936], based on 5 years of temperature measurements in the southern part of Monterey Bay, characterized the duration of the upwelling period as extending from March through August, with September–October constituting what he termed the oceanic period. The oceanic period was marked by the warmest surface temperatures (found in September) and exhibited marked stratification in the vertical. *Bolin and Abbott* [1963] examined data collected weekly throughout 1954–1960 at six stations distributed mainly across the mouth of the bay. They noted that the surface temperatures during the upwelling period were marked by a greater degree of spatial variability than was found during the oceanic period. The near homogeneity of the near-surface (3 m) temperature and salinity fields at this time of year is confirmed by the data shown by *Rosenfeld et al.* [1994b]. Any persistent horizontal structure in the surface

temperature and salinity fields is minimal, with average temperatures generally in the 14°–15°C range and average salinities between 33.37 and 33.52.

Breaker and Broenkow [1994], in a recent review of the circulation of Monterey Bay, refer to an engineering report [*Brown and Caldwell Engineers*, 1979] which shows predominantly westward flow during June–September 1976 at 9-, 15-, and 25-m depth in 30 m of water off Santa Cruz at the northern end of Monterey Bay. Two days worth of drifter and CTD data from August 1972 [*Moomy*, 1973] indicate cyclonic circulation within the bay.

The California Cooperative Oceanic Fisheries Investigations (CalCOFI) data set has been used by several authors [*Hickey*, 1979; *Wyllie*, 1966; *Chelton*, 1984; *Lynn and Simpson*, 1987] to calculate the geostrophic velocity field in the California Current region. Although an excellent data set for many purposes, the limited coverage over the continental shelf and upper slope makes it less than ideal for estimating flow past the mouth of Monterey Bay [*Chelton et al.*, 1987]. More closely spaced CTD stations off Point Sur, just south of Monterey Bay, showed the nearshore geostrophic flow to be poleward during a period of calm winds in August 1988 [*Tisch et al.*, 1992]. Surface drifters deployed north and south of Monterey Bay, and tracked only by their recovery position, showed no preferred direction of flow in August 1972 [*Griggs*, 1974]. Drifters drogued at 50 m showed flow to be poleward and seaward past the Monterey Peninsula over several days in August 1972 and 1973 [*Wickham*, 1975]. The existing data are such that no prediction can be made with confidence of the prevailing near-surface current patterns in this region for the August–September time frame.

Although the monthly mean winds are near zero at this latitude during fall and winter [*Nelson*, 1977; *Strub et al.*, 1987], the low-frequency winds are more variable than in spring and summer. By October the upwelling-type circulation described previously occurs much less frequently, and near-surface flow along the central coast is under the influence of the northward flowing Davidson Current, which generally reaches its maximum speed at the surface in December [*Chelton*, 1984]. *Tisch et al.* [1992] found poleward geostrophic flow throughout the water column in a narrow band inshore of the anticyclonic eddy in November 1988 off Point Sur. The following November they found weak equatorward flow next to the coast, inshore of the poleward flowing Davidson Current. The Central California Coastal Circulation Study conducted during February 1984 to July 1985, found the flow direction between Point Año Nuevo and Point Conception to be variable in October, but by January the Davidson Current was well established south of Point Sur, though less so to the north of there [*Chelton et al.*, 1987]. Some brief near-surface parachute drogue measurements made in the Point Sur to Cape St. Martin area in October 1958 and January 1959 are consistent with weak poleward surface flow in October and stronger poleward flow in December [*Reid and Schwartzlose*, 1962]. *Griggs's* [1974] drifters show the dominant flow direction in Monterey Bay to be northward during November–February 1971–1972 and 1972–1973. We know of no direct time series measurements of the near-surface wintertime currents in the outer part of the bay other than those from the CODAR and moored self-contained ADCP, some of which are presented in this paper.

In summary, what we know about near-surface currents in the vicinity of Monterey Bay includes the following: in spring through midsummer (roughly March–July) we expect the flow to be equatorward past the mouth of the bay in the mean; in August–September the flow is probably weaker and more variable in direction; in October the poleward flowing Davidson Current spins up (or the California Undercurrent shoals), at least along the coast south of Monterey Bay, reaching its maximum speeds in December–January. This summary description falls between those for the seasonal cycles of alongshore currents at 35-m depth over the shelf to the north (39°N) and south (35°N) of Monterey Bay presented by *Strub et al.* [1987] based on current meter measurements made during 1981–1983.

2. Data and Methods

Based primarily on the availability of CODAR measurements, we concentrate on a description of the late summer time frame using data from 1992 and 1994. (There are no CODAR data for 1993.) While we discuss circulation patterns from both years, comparisons with moored observations (described below) are performed only for 1994 because the CODAR range often did not include the mooring site during 1992.

2.1. CODARs Around Monterey Bay

Two CODAR systems owned by NOAA were installed on the shores of Monterey Bay in 1992. One was placed at the Hopkins Marine Station near Monterey at the south end of the bay, and the other was placed at the Monterey Bay Aquarium Research Institute (MBARI) facility in Moss Landing, half way around the bay to the north (Figure 1). These instruments were older-generation CODAR units. They operated at a frequency of 25.4 MHz, which resulted in a resonant wavelength for the Bragg scatterers of 5.9 m. The data coverage from these systems extended over the southern two thirds of Monterey Bay with typical ranges of 25 km. Results from the two-site array were analyzed for the 3-month period March through May 1992 [*Neal*, 1992] and the 1-month period of September 1992 [*Foster*, 1993] with particular focus on the low-frequency surface currents and the influence of the daily sea breeze. Tidal period surface currents for September 1992 were also analyzed [*Petruncio*, 1993].

In 1993 and 1994 the HF radar array around Monterey Bay was augmented by three SeaSonde systems: (1) a unit purchased and installed south of Monterey Bay by Stanford University at the Granite Canyon Marine Laboratory, (2) a unit purchased and installed by the Naval Postgraduate School at Point Pinos at the southern tip of Monterey Bay, and (3) a unit purchased and installed by NOAA at Long Marine Laboratory in Santa Cruz at the north end of Monterey Bay (Figure 1). The SeaSonde systems operated at frequencies near 12.5 MHz, which resulted in a resonant wavelength for the Bragg scatterers of 12.0 m. The hypothetical coverage areas for each of the individual radar units are outlined in Figure 1 along with the locations of moored current and wind observations. (The achieved coverage area for the 1994 observations is discussed below based on actual data returns.)

After the installation of the SeaSonde system at Point Pinos the older-generation CODAR system at the Monterey site was decommissioned and used to provide spare parts for the system in Moss Landing. Therefore the radar array in 1994 consisted of the two SeaSonde sites at Point Pinos and Santa Cruz plus the older-generation CODAR site at Moss Landing. (We do not use data from the Granite Canyon SeaSonde in this study.)

Radial current data from individual radar sites were combined to produce vector current maps every 2 hours. This time

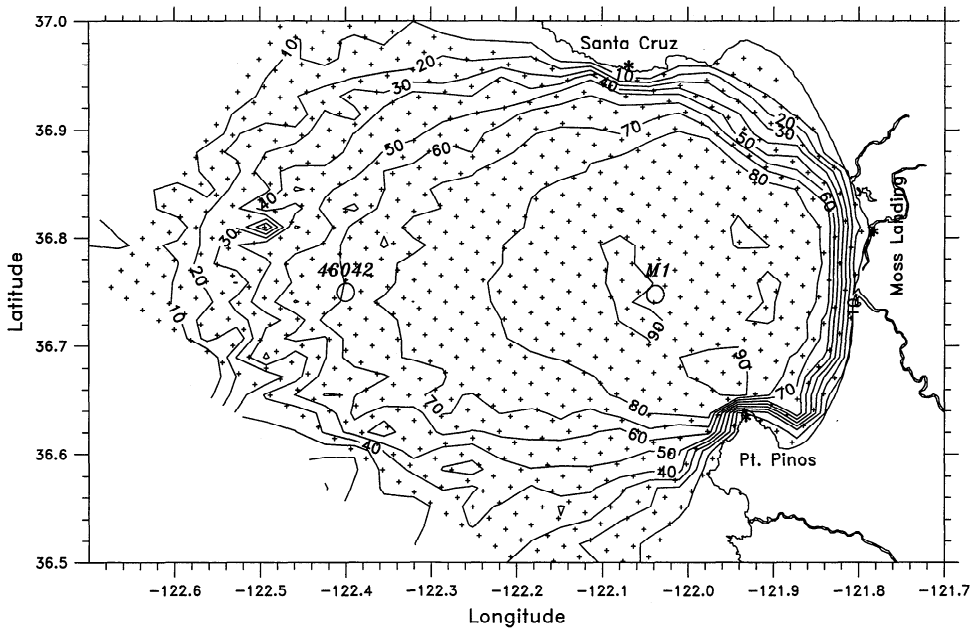

Figure 2. Percent temporal coverage of possible 2-hourly radar-derived current vectors for the period August–December 1994. Symbols denote locations of current vector grid points (plusses) and watch circles of the two moorings used in this study (open circles).

interval was set by the speed of the older CODAR units, which collected backscatter data over a 30-min period and required about 90 min to process the results. The SeaSonde systems collected backscatter data continuously and computed radial currents based on a running average over 60 min. The vector-processing step was conducted by the manufacturer of the radar systems under contract to NOAA. Maps were produced by first defining a regular grid throughout the maximum possible coverage area. Vector estimates were then attempted for each grid location using a least squares vector fit [*Lipa and Barrick*, 1983; *Gurgel*, 1994] applied to all radial data within a radius of 3 km. (It is our longer-term goal to improve on the vector mapping technique. However, we use the processed vector currents as the "raw" data in this study.)

Vector time series for a particular radar bin will have gaps at times when there were insufficient radial observations nearby to estimate the vector current. Gaps in radial observations were produced when one or more radar sites were down. In addition, radial data can have spatial and temporal gaps (even when all systems are operating) for two reasons: (1) the direction finding algorithms cannot always resolve all angular directions for a given range cell, and (2) maximum range fluctuates. The first reason is unique to CODAR-type HF radars, but the range fluctuation is common to all HF radars. The maximum range is variable because signal to noise ratios depend on several factors, such as sea state and antenna conditions. A systematic fluctuation in range due to diurnal variations in atmospheric conditions has been pointed out by *Prandle et al.* [1993]. In Monterey Bay this diurnal range variation is observed to be about 3 km with maximum range occurring in the evening and minimum range occurring around noon.

To characterize the availability of data from the three-site configuration and to provide a crude measure of the reliability of the data from different regions, we investigated the data returns over long time periods as a function of location. The data coverage for the 5-month period of August through December 1994 is summarized in Figure 2, which shows the percentage of time velocity estimates were obtained at each radar bin. Figure 2 can be used to assess the useful range of the three-site radar network because both the number of data gaps at a given location and the reliability of data from that location can be expected to scale with the percent coverage. We use the 50% coverage contour as the nominal limit of useful HF radar data because the coverage drops quickly beyond this region. We note that very few of these data gaps were produced by radar down time because all three sites were in operation during most of the study period, with the exception of several days when only two sites were in operation and a 4-day period beginning 28 August when all three sites were down.

2.2. Moored Acoustic Doppler Current Profiler (ADCP) and Wind Observations

MBARI has maintained a surface mooring, designated M1, at approximately 36.75°N, 122.02°W since August 1989 (Figures 1 and 2). A 150-kHz RD Instruments SC-ADCP has been deployed on this mooring in a downward looking configuration since January 1992. Data from the third deployment are used here. The instrument was set up with an 8-m pulse length, 8-m bin length, and 4-m blanking. The transducers sit 1 m below the waterline. Therefore the top bin, which we will be comparing to the CODAR data, is centered at 9 m. Two orthogonal components of horizontal velocity are derived from the Doppler shift along four beams aligned at 30° to the vertical in a Janus configuration [*RD Instruments*, 1989]. Every 15 min, data from 110 pings at 1-s intervals were averaged together. The manufacturer's quoted accuracy for this configuration is 1.2 cm s^{-1}. These ensembles serve as the raw data set, which was transmitted to MBARI every few hours via packet radio. These data were then low-pass filtered with a cosine-sinc filter with the half-amplitude point at 36 hours to isolate subtidal motions.

The M1 mooring position is monitored by onboard Global

Positioning System (GPS) receivers. Mooring position was determined from a 2-min average every 30 min. During the third deployment, including August–December 1994, a five-channel Magellan receiver was used, with 0.01′ resolution. The average standard deviation and number of independent samples for the position estimates are 40 m and 113, respectively, giving an average standard error (defined in section 4) for each mean position of 7.5 m. Thus mooring velocity estimates are expected to be accurate to slightly better than 1 cm s^{-1} (15 m (30 min^{-1})). Mooring velocities were low-pass filtered in the same way as the observed currents and added to the SC-ADCP velocities in order to remove the effect of mooring motion from that data. This represents a small correction of ~1 cm s^{-1} for subtidal velocities. Most of the mooring motion is in response to diurnal and semidiurnal current or wind fluctuations.

The MBARI mooring M1 supports RM Young propeller/vane wind sensors at a height of 3.8 m above sea level. Wind data on this mooring are sampled at 2 Hz for 1 min out of every 10 and averaged [*Hayes*, 1989]. In addition to this MBARI mooring the National Data Buoy Office maintains a meteorological mooring numbered 46042 at 36.75°N, 122.41°W with wind measurements at 5.0 m above sea level (Figures 1 and 2). For this study we use the 10-min wind observations from M1 and hourly (8-min average per hour) wind data from buoy 46042 for comparison with radar-derived currents. Cross-spectral or correlation analyses are conducted using an estimate of wind stress given by $\boldsymbol{\tau} = \rho C_D |\mathbf{w}| \mathbf{w}$, where C_D and ρ are constant drag coefficients and air densities, respectively.

2.3. Vessel-Mounted ADCP Observations

Over the course of a 19-hour period on August 6–7, 1994, an east-west line along 36.63°N off the Monterey Peninsula was transited four times. The section extended approximately 30 km offshore from Point Pinos. A 150-kHz ADCP mounted in the hull of the R/V *Pt Sur* was operated continuously during this period to collect current profiles along the transect. The pulse length, bin length, and blanking intervals onboard the ship matched that of the SC-ADCP set-up at M1. The transducers were 3 m below the surface; thus the top bin was centered at 11 m. The vessel-mounted (VM)-ADCP formed averages over 180-s intervals, which contained anywhere from 96 to 177 pings, with an average of 128. Sound speed corrections were made based on the measured temperature. A calibration run with bottom tracking was made during the 5-day cruise, and velocity data were corrected for gyro and alignment error using the method of *Joyce* [1989]. The ship's velocity, calculated from navigation information acquired with a differential GPS system, was subtracted from a reference layer velocity calculated as the average velocity over bins 3–5. This absolute reference layer velocity was then gap filled, despiked, and smoothed with a cosine-sine filter of width 27 min. The vertical profiles were then adjusted to the reference layer. (Taking into account instrument, alignment, and navigation errors, we estimate the accuracy of the resulting data to be ±3 cm s^{-1}.) Finally, the 3-min processed data from all four transits were averaged together into 2-km bins to match the spatial resolution of the radar-derived currents.

A similar vessel-based data set was collected along two 8-km transects during October 29–31, 1994. One section was centered along the Monterey Submarine Canyon near its head and the other section was cross-canyon in the same area. The measurements each covered 25-hour periods and were conducted as part of a study of internal tides in the canyon. Processing of VM-ADCP currents during this experiment was similar to that described above for the August transect, including averaging of the upper level currents into 2 km along-track bins to match the spatial resolution of the radar-derived currents.

2.4. Drifting Buoy Observations

Two separate drifter experiments were conducted in which a group of satellite-tracked surface drifters were deployed within the coverage area of the HF radar network, as detailed by *Paduan et al.* [1996]. The first experiment took place during August 20–22, 1992, and the second took place during October 29–31, 1994. The 12 drifters deployed during the first experiment were all of a single design, the Argosphere. It consists of a 30-cm-diameter fiberglass sphere containing batteries, an antenna, and an Argos transmitter. These instruments were produced to follow spilled oil floating on the water surface, and tests have shown them to follow oil slicks accurately for several days [*Reed et al.*, 1990]. The undrogued surface sphere is expected to have a large downwind component that could differ significantly from the water motion in the upper 1 m.

The drifters deployed during the second experiment were of two designs: (1) fiberglass spherical floats similar to the Argosphere drifters, but tracked by a combination of GPS and Argos, and (2) Coastal Ocean Dynamics Experiment (CODE)-type drifters tracked by Argos. The CODE-type drifters consist of a 1-m-long PVC tube containing an Argos transmitter and batteries. Attached to the tube are four rectangular drogue elements arranged in a cross and suspended by small Styrofoam floats. The instruments were designed to follow the motion of the upper 1 m of the water column with minimum coupling to surface waves or wind [*Davis*, 1985]. A total of six GPS and five CODE-type drifter deployments were made in this experiment.

3. Comparisons With In Situ Observations

In this section we compare radar-derived surface currents with in situ observations. As with all other remote sensing techniques it is not possible to obtain direct measurements over the same space scales and timescales or depths using in situ instrumentation. This point cannot be overstated. It is particularly important when comparing HF radar-derived surface currents and more traditional in situ measurements. The radar estimates are averages over some 4–10 km^2 and 30–60 min. Even more to the point, the radar estimates represent average currents in the upper 1–2 m of the water column. Moored current meters and ADCPs and VM-ADCPs all suffer from significant error sources within the upper few meters of the water column due to factors like Stokes drift and bubble injection. Well-designed surface drifters may measure very near-surface currents with small errors, but they cannot provide space scale and timescale sampling comparable to HF radar.

Despite inherent scale and depth mismatches it is possible to verify many aspects of radar-derived currents using in situ measurements. For example, high correlation can be expected between radar-derived currents and deeper moored current observations for low-frequency, large-scale fluctuations. However, this requires long time series observations from both the remote and in situ systems. Similarly, tidal-period fluctuations, which are phased locked over long periods and coherent over large depth ranges, can be expected to show coherence between radar-derived currents and deeper moored current observations. Again, long time series observations are required to

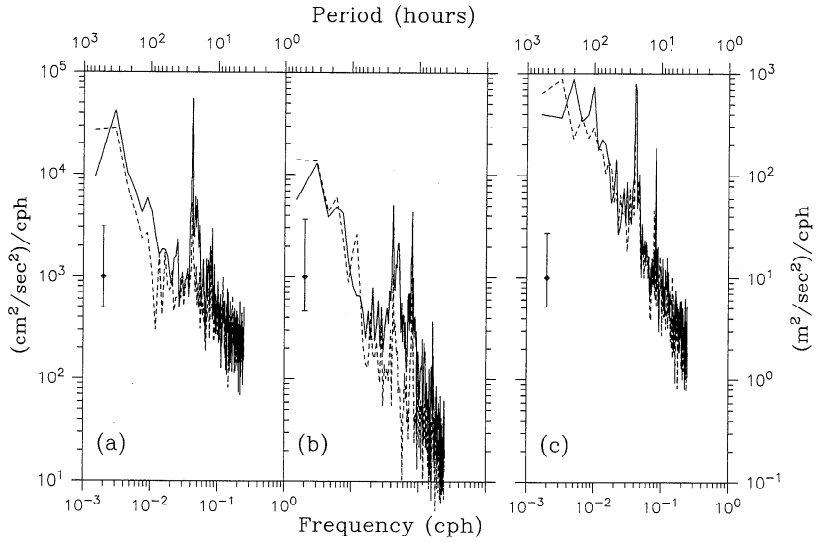

Figure 3. Rotary frequency spectra for (a) radar-derived current at grid point 1214 on the western edge of the M1 mooring watch circle, (b) ADCP currents at 9 m on the mooring, and (c) winds at 4 m above the mooring. Both clockwise (solid lines) and counterclockwise (dashed lines) energy levels are shown, as are the 95% confidence limits for the companion one-sided autospectra.

extract the tidal signal. A counterexample may be high-frequency wind-driven surface currents, such as those responding to diurnal sea breeze forcing, which may be expected to differ significantly for radar measurements at 1 m and moored current observations at, say, 10 m. It is with these important physical insights in mind that we attempt to characterize the radar-derived currents by comparing them with moored current and wind observations, ship-based current observations, and drifter-derived currents.

3.1. Moored Current and Wind Observations

The moored instrumentation at site M1 provides us with long time series measurements of currents and winds, which can be compared with the radar-derived currents in the vicinity of the mooring. The M1 location at the mouth of Monterey Bay is an area with good HF radar coverage (Figure 2). In this study we exploit the period of maximum overlap between in situ observations and radar-derived currents. Winds and radar-derived currents are compared for the 5-month period August through December, 1994. Moored ADCP current records terminate on November 21, which gives a shorter overlap period of just under 4 months. The watch circle of the M1 mooring lies between the center points of three radar bins (Figure 2). In the time domain we compare mooring data with radar-derived currents averaged over the three bins surrounding the mooring site. Spectral calculations are shown for the single radar bin centered just west of the watch circle, although results from the other nearby bins are similar. Gaps in the various time series are rare and, usually, less than 12 hours in duration. These short gaps were filled using linear interpolation. Spectral calculations were made using data segments that avoid the 4-day gap beginning August 28.

Rotary spectra are used to identify the frequency bands dominating the current (or wind) fluctuations. These computations combine spectral information in the east-west (u) and north-south (v) fluctuations into clockwise and counterclockwise-rotating fluctuations [*Gonella*, 1972]. In order to avoid large gaps in the time series and to improve the statistical description of the fluctuations, we compute spectral estimates over 25- to 28-day segments and average the results for the August through December period. This gives four to six total segments and eight to 12 degrees of freedom in each spectral band, depending on the data type. Rotary spectra for radar-derived currents, ADCP currents, and winds at or near the M1 mooring location are shown in Figure 3. Spectral characteristics of the currents are similar for the radar-derived and ADCP time series. Both data sets exhibit a significant spectral gap between low-frequency motions with periods greater than 4 days and energetic motions around the diurnal period. Low-frequency motions in the radar data are slightly more energetic than those in the ADCP data, but neither data set shows significant polarization at low frequencies.

Significant peaks exist in the current measurements around the diurnal and semidiurnal periods. The diurnal peak, in both cases, extends across the diurnal to inertial frequency band from periods of 24–20 hours. There is a suggestion of two separate peaks at these frequencies, but they are barely resolved with the segment lengths used here. The entire diurnal/inertial band is polarized with at least an order of magnitude more energy in the clockwise-rotating fluctuations. The energy level of the inertial peak at 20 hours is similar in both data sets, but the diurnal peak is an order of magnitude larger in the HF radar time series, which is consistent with strong diurnal wind forcing affecting the currents at 1-m depth much more than those at 9 m [*Foster*, 1993; *Petruncio*, 1993]. Fluctuations at semidiurnal periods are slightly more energetic in the ADCP data than in the HF radar data. These motions are believed to be due to baroclinic tidal currents [*Petruncio*, 1993]. The rotary spectrum of wind fluctuations at the M1 mooring exhibits a consistent roll off proportional to $f^{-3/2}$, where f is the frequency. There are two notable exceptions to this simple red spectrum. Sharp peaks exist in the wind spectrum at diurnal/inertial and semidiurnal periods.

To investigate correlation at low frequencies among the radar-derived and SC-ADCP currents and buoy winds, we low-pass filtered the time series with a 36-hour half-amplitude point cosine-sinc filter. The filtered time series of radar-

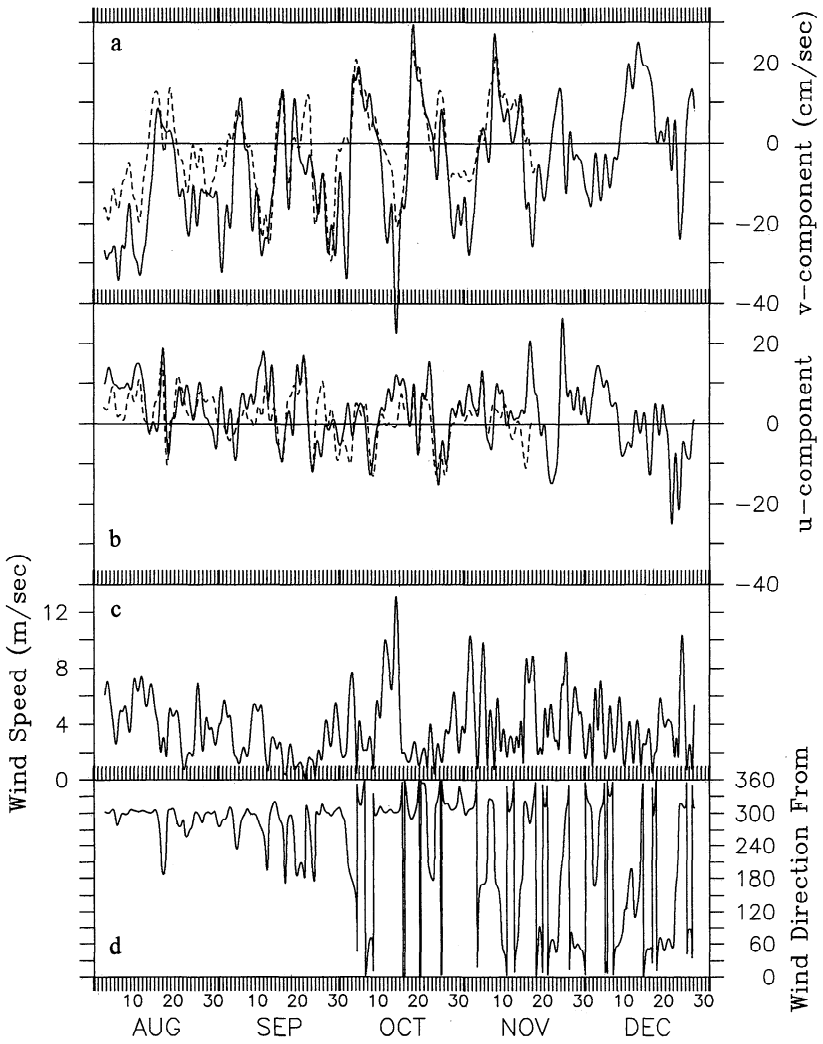

Figure 4. Low-pass-filtered (a) v and (b) u velocity components from the average of three radar bins around the M1 mooring (solid lines) and from the ADCP bin centered 9 m below the mooring (dashed lines) in 1994. Low-pass-filtered (c) wind speed and (d) direction are also shown.

derived currents at 1 m, ADCP currents at 9 m, and wind 4 m above the surface are shown in Figure 4 for the August through December period. The ADCP data, which have been corrected for mooring motion using the GPS position of the surface float, end in late November when the instrument was removed for maintenance. During the overlap period, there is obvious visual correlation between the filtered radar-derived currents and ADCP currents. The root mean square (rms) differences are 6.2 cm s^{-1} and 10.8 cm s^{-1} for the u and v components, respectively, and 50.6° for direction. In the v direction, strong current fluctuations are observed at this location with timescales of about 2-weeks in both data sets. Currents are weak or equatorward early in the records, but beginning in October the currents exhibit sustained periods of poleward flow.

The complex correlation between the remotely sensed surface currents in the vicinity of the M1 mooring and the ADCP currents and wind stress on the mooring is shown in Figure 5 as a function of time lag. The magnitudes and phases of the correlations are shown for lags up to 24 days. *Kundu* [1976] illustrates how the magnitude of the complex correlation coefficient provides a measure of the traditional covariance of the vector components over time, while the phase gives the average difference in the direction of the two vectors over the same period. The correlation magnitudes at zero lag are large, with values of 0.79 and 0.56 for radar-derived and ADCP current and the radar-derived current and wind stress comparisons, respectively. The correlations are maximum at zero lag and drop significantly for lags of just a few days. Secondary correlation peaks of about 0.3 occur, however, for positive and negative lags at multiples of about 17 days. This is true for both the current-current comparisons and current-wind stress comparisons. It is a result of the strong events in the v currents that occur with surprising regularity in the time period of these observations. Much of the variance in the 4- or 5-month current records is accounted for by these nearly periodic events so that shifting one time series relative to the other by a multiple of about 17 days produces relatively large correlation. In both the current-current and current-wind stress cases the correlation of scalar components (not shown) is higher for v motions than it is for u motions: for the current-current comparisons the zero lag correlations are 0.58 and 0.83 for the u-u and v-v components, respectively; for the current-wind stress comparisons, the zero lag correlations are 0.35 and 0.48 for the u-τ^x and v-τ^y components, respectively. These and other correla-

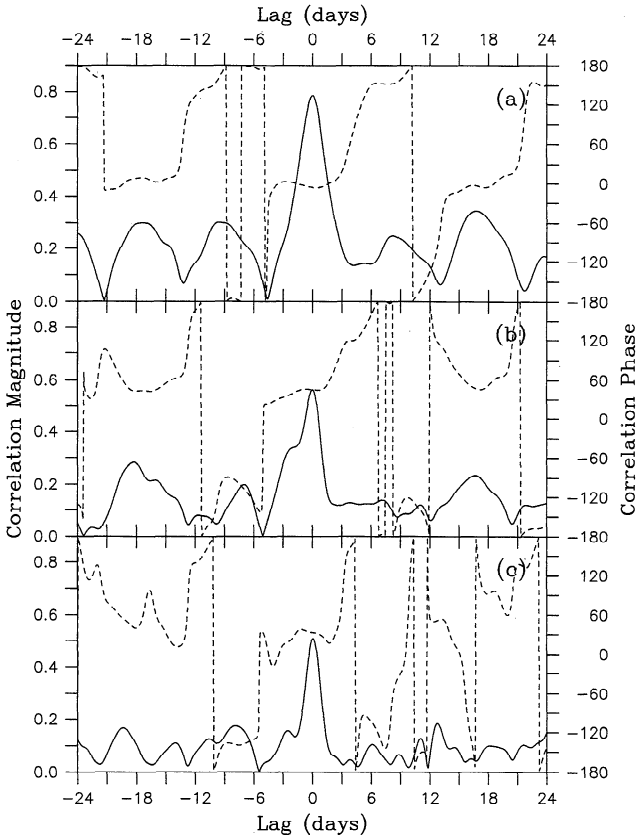

Figure 5. Lagged complex correlation magnitude (solid lines) and phase (dashed lines) based on low-pass-filtered time series (a) between radar-derived currents around the M1 mooring and ADCP currents 9 m below the mooring, (b) between radar-derived currents around the M1 mooring and wind stress above the mooring, and (c) between radar-ADCP velocity difference and wind stress.

tion results are summarized in Table 1 along with the rms differences.

To assess the significance of these linear correlation coefficients, we must determine the independence timescales for the dominant processes in the time series. With this information we can compute the number of independent samples in the correlations and the likelihood that the observed correlations exceed random chance. A measure of the independence timescale is given by the autocorrelation functions for low-pass-filtered velocity and wind stress time series. These functions are shown in Figure 6 for the radar-derived and ADCP currents and wind stress. We use the e-folding values to estimate integral timescales. For each data type the timescale for v motions is longer than that for u motions. Values for the radar-derived and ADCP currents are similar to each other, while values for the wind stress time series are shorter. Longer estimates provide the more conservative statistical interpretations. Hence we use estimates of 36 hours and 72 hours for u and v motions, respectively, for all data types. The velocity-velocity correlations above are based on time series over 2700 hours. This yields some 76 or 38 independent estimates of the low-frequency motions based on the u and v timescales, respectively. Correlation values >0.23 (0.32) have less than 5% probability of deriving from a random sample given 76 (38) independent comparisons [*Bevington*, 1969]. The radar-derived currents and wind stress correlations extend over 3700 hours, yielding 100 or 50 independent estimates. Correlation values >0.20 (0.28) have less than 5% probability of deriving from a random sample given 100 (50) independent comparisons.

Although low-frequency fluctuations in radar-derived and ADCP currents are highly correlated, the agreement is not uniform throughout the overlap period. The times of largest velocity differences between the two series are correlated with the times of largest winds (compare Figure 4). The complex correlation between radar-ADCP velocity difference and wind stress (Figure 5) is significant. The magnitude at zero lag is 0.51 and the phase difference is 32.6° with velocity difference to the right of wind stress. In contrast to this, velocity difference is only weakly correlated with temperature difference between 1 m and 20 m measured on the mooring (Table 1). Velocity shear may be expected to correlate with wind forcing near the surface. However, it is also true that the radar-derived currents include a Stokes drift component that is not present in the ADCP currents [*Barrick*, 1986]. Since this wave-induced component is proportional to wind stress, it is reasonable to expect Stokes drift to account for some of the observed difference between radar-derived and ADCP currents, particularly given the low correlation with near-surface stratification. Although we do not have direct measurements of the wave heights needed to quantify this effect, we note that Stokes drift at the surface could be as large as 3 cm s^{-1} for the Bragg wavelengths

Table 1. Summary of Correlation, Rms Differences, and Median Differences Between Radar-Derived Currents and In Situ Data or Between Radar-ADCP Current Shear at the M1 Mooring and In Situ Data

	Measurement Depth, m	Correlation u:u, v:v (95%)	Correlation Magnitude (Phase)	Rms Difference u-u, v-v (Angle), cm s^{-1}	Median Difference u-u, v-v (Angle), cm s^{-1}
		Between Radar-Derived Currents and In Situ Data			
HF radar	−1	...	...	...	...
Moored ADCP	−9	0.58, 0.83 (0.23, 0.32)	0.79 (−6.3°)	6.2, 10.8 (50.6°)	3.9, 6.7 (20.0°)
Moored wind stress	4	0.35, 0.48 (0.20, 0.28)	0.56 (45.3°)	...	...
Drifting buoy	−1	0.37, 0.73 (0.20, 0.20)*	0.58 (0.0°)	16.2, 13.6 (63.7°)	9.5, 8.3 (36.1°)
VM-ADCP	−11	−0.25, 0.45 (0.46, 0.46)*	0.32 (46.1°)	13.2, 8.4 (60.3°)	10.1, 4.5 (53.6°)
		Between Radar-ADCP Current Shear at M1 Mooring and In Situ Data			
$\Delta(u, v)/\Delta z$:wind stress	...	0.39, 0.48 (0.23, 0.32)	0.51 (32.6°)	...	...
$\Delta(u, v)/\Delta z$:$\Delta T/\Delta z$	...	−0.31, 0.01 (0.23, 0.32)	0.18 (−178.7°)	...	...

Time series data at or near the M1 mooring were low-pass filtered as described in the text. Drifter- and ship-based measurements were compared directly with the closest radar observation. Measurement depths give nominal height above the sea surface for each data type.

*These significance levels assume each radar/drifter or radar/VM-ADCP pair is independent.

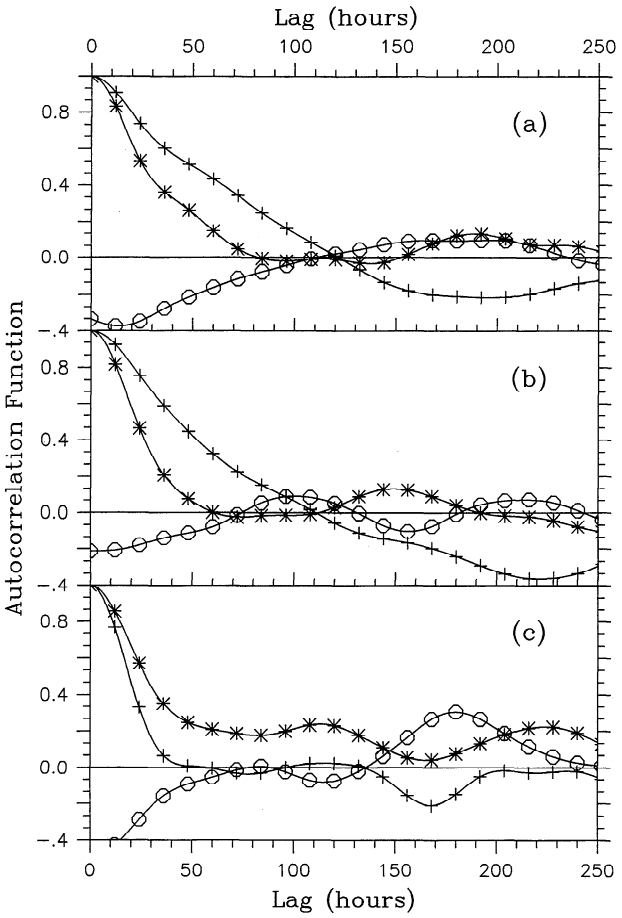

Figure 6. Lagged correlation functions for u-u (asterisks), v-v (plusses), and u-v (open circles) based on low-pass-filtered time series of (a) radar-derived currents around, (b) ADCP currents 9 m below, and (c) wind stress above the M1 mooring.

in question assuming an upper bound of 10 cm for the wave amplitude [*LeBlond and Mysak*, 1978].

In the case of the correlations between radar-derived currents and measured wind stresses, computing the complex correlation increases the overall correlation. This is because the radar-derived current and measured wind stress vectors are highly correlated but not, on average, pointed in the same direction. This is also shown by the phases of the complex correlations at zero lag, which are −6.3° and 45.3° for the current-current and current-wind stress comparisons, respectively. These results show that at subtidal frequencies, the radar-derived currents are correlated with both the ADCP currents 9 m below and the wind stress 4 m above the surface. The radar-derived currents are in nearly the same direction as the ADCP currents at these frequencies. The current direction is seen to be, on average, 45° to the right of the wind direction, which is consistent with classical Ekman theory for steady state wind-driven motions.

Crosby et al. [1993] proposed an alternate formulation for the calculation of vector correlations (see also *Breaker et al.* [1994] for applications to geophysical vector data). Their method represents a more general extension of the scalar correlation than does the method of *Kundu* [1976] and, as such, has many desirable statistical properties. The formulation does not, however, provide both magnitude and angle information. For our study the alternate vector correlation between radar-derived currents and moored ADCP currents is 0.51, where we have normalized the range to fall between 0 and 1. The alternate vector correlation between radar-derived currents and wind stress is 0.20. Both of these comparisons are highly significant at the 95% level, assuming a minimum of 38 and 50 independent observations for the current-current and current-wind stress comparisons, respectively [*Crosby et al.*, 1993]. The alternate vector correlation between radar-ADCP velocity difference and wind stress is also significant at 0.22.

All correlations described here represent time domain analyses that combine fluctuations at all frequencies in order to determine how much of the total variance is common to both time series. It is also possible to investigate the frequency-dependent coherence between radar-derived currents and ADCP currents or wind based on the cross spectrum of two complex time series [*Gonella*, 1972; *Mooers*, 1973]. The coherence squared and phase between radar-derived currents and ADCP currents and between radar-derived currents and winds are shown in Figure 7. Results are shown for both positive (counterclockwise) and negative (clockwise) frequencies with frequency increasing from the center of the figure outward to the sides. The cross-spectral calculations were conducted by ensemble averaging the results obtained from 25-day or 28-day data segments and band averaging the results at high frequencies. The dotted lines show the coherence squared level at which the results are known to be significantly different from zero with 95% confidence. The cross-spectral results are noisy but generally support the conclusions drawn from the correlation analyses: there is significant coherence across the subtidal frequency band and at the tidal/inertial frequencies where energies are high in the individual time series (compare Figure 3). Furthermore, the phase differences tend to cluster around zero for the current-current case and −45° for the current-wind case at those frequencies where coherences are high. The negative angles in the current-wind phase differences indicate that for both clockwise and counterclockwise-rotating currents and winds, current vectors are to the right (clockwise) of the wind vectors.

For comparison with the above results the coherence squared and phase between ADCP currents and winds are also shown in Figure 7. For this case, coherence levels are low everywhere except at the inertial frequency. In general, ADCP-measured currents at 9 m on the M1 mooring are less coherent with winds directly above them than are radar-derived currents at 1 m in the vicinity of the mooring. This can be attributed to depth differences, Stokes drift in the radar-derived currents, and the fact that the shorter ADCP time series have less statistical opportunity to verify significant coherences in the presence of noise (we use four segments of 28-day length for cross spectra involving ADCP records but six segments of 25-day length for the radar-derived current and wind cross spectrum due to the different record lengths and the timing of the long 4-day gap in the radar data).

Wind observations from the 46042 mooring were not compared directly with radar-derived currents at that location because the temporal coverage there was only 60% (Figure 2). Instead, comparisons were made between low-pass-filtered wind stress from the 46042 and M1 mooring locations as a check on the horizontal length scales in the wind observations. Complex correlation of wind stress between the two sites was very high: the correlation magnitude was 0.87 and the average direction difference was 11.9°. As would be expected with this

degree of wind correlation, radar-derived currents around the M1 mooring were found to correlate with wind stress at 46042 nearly as well as they do with wind stress directly overhead.

3.2. Ship-Based Current Observations

The comparison of radar-derived currents and moored ADCP currents at the M1 site shows that correlation between these different measurement systems can be expected for subtidal motions. Away from the M1 site we lack the moored time series measurements required to confirm this expectation. However, additional comparisons with in situ measurements are available from the two ship-based experiments in which VM-ADCP current observations were made repeatedly over the same track during a 19- or 25-hour period. The average radar-derived and VM-ADCP current vectors for August 6 are plotted together with the sea surface temperature from the single AVHRR satellite pass at 0300 UT in Plate 1. The VM-ADCP current vectors represent an average over four passes made during a 19-hour period. The radar-derived current vectors are an average of twelve 2-hourly maps centered on the ship observations. The currents as measured by these two systems show many similarities. Observations nearest to the northwest tip of the Monterey Peninsula show weak mean currents. Further offshore the flow is equatorward at about 15 cm s^{-1} in the VM-ADCP observations at 11 m and southwestward at about 20 cm s^{-1} in the radar-derived currents. The consistent direction bias of 56° between the two measurement systems during this period is unexplained. It is opposite to the rotation with depth expected in an Ekman layer. The temperature data are consistent with the features seen in the radar-derived surface currents, particularly the equatorward current extending across the mouth of Monterey Bay.

Current observations averaged over two 12-hourly repetitions of along and cross-canyon transects during October 1994 are shown together with the 24-hour average radar-derived currents in Figure 8. Here the average current magnitudes are very weak (<5 cm s^{-1}) from both measurement systems. Mean current directions are consistently southwestward during the cross-canyon transect period in both types of measurement, but they vary from bin to bin in both types of measurement during the along-canyon transect period.

Radar versus VM-ADCP correlations and rms differences were computed over the relatively small data set presented in Plate 1 and Figure 8. Each available 19- or 25-h VM-ADCP vector was paired with the closest radar vector averaged over a similar time period. (The densely spaced VM-ADCP vectors in Figure 8 were first averaged spatially to simulate the nominal 2-km spacing of the radar data.) This yielded a total of 19 velocity pairs, which were assumed to be independent. The correlations between these velocity pairs are not statistically significant (Table 1), although the phase of the complex correlation does reflect the direction bias seen in Plate 1. The rms differences for this data set are 13.2 cm s^{-1} and 8.4 cm s^{-1} for the u and v components, respectively. The rms speed difference is 10.6 cm s^{-1} and the rms direction difference is 60.3°.

3.3. Surface Drifter Observations

Surface current estimates from the drifter deployments and HF radar were compared by pairing the closest-in-time and closest-in-space radar-derived vector with each drifter-derived vector. A detailed breakdown of these results is given by *Paduan et al.* [1996], including the statistical comparisons and

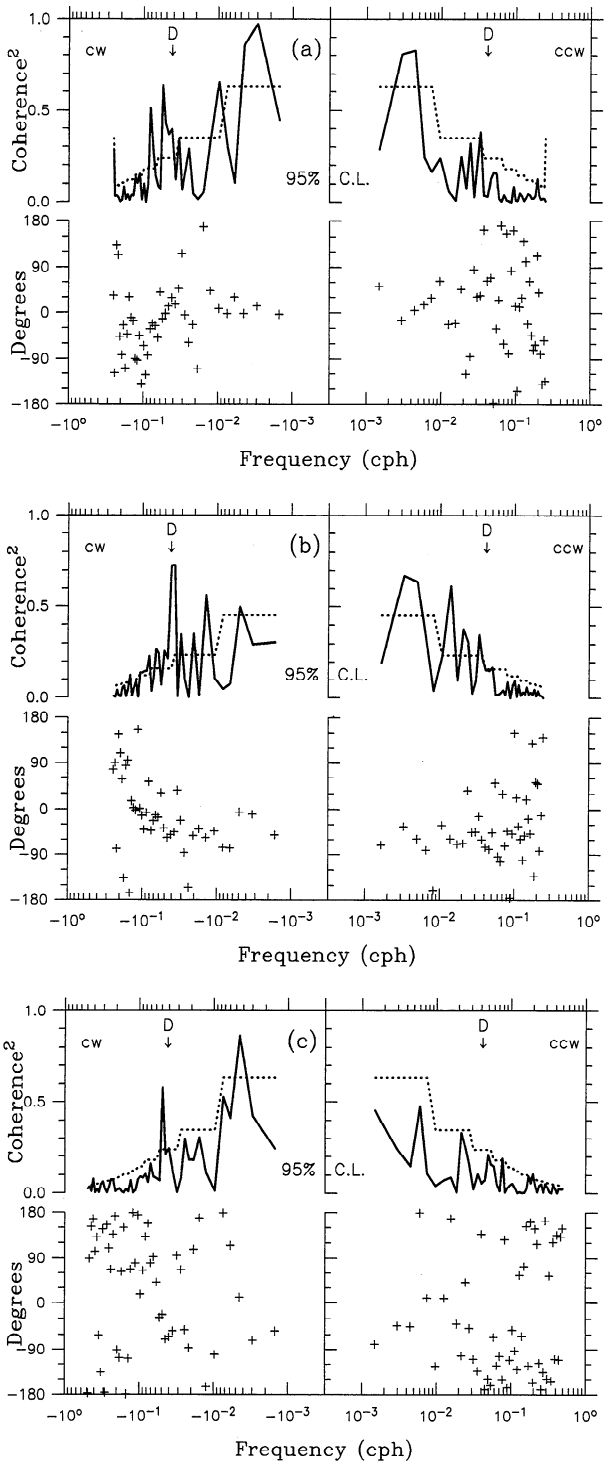

Figure 7. Coherence squared and phase as function of frequency for the ensemble-averaged and band-averaged cross spectra between (a) radar-derived currents at grid point 1214 near the M1 mooring and ADCP currents 9 m below the mooring, (b) radar-derived currents at grid point 1214 and wind velocity 4 m above the mooring, and (c) ADCP currents 9 m below the mooring and wind velocity 4 m above the mooring. Negative phase values denote current to the right of the rotating wind vector or ADCP currents to the right of the rotating radar-derived current vector for both clockwise (cw) and counterclockwise (ccw) motions. Frequency increases from the center of the figures outward to the sides. The spectral locations of diurnal period fluctuations (D) are shown for reference.

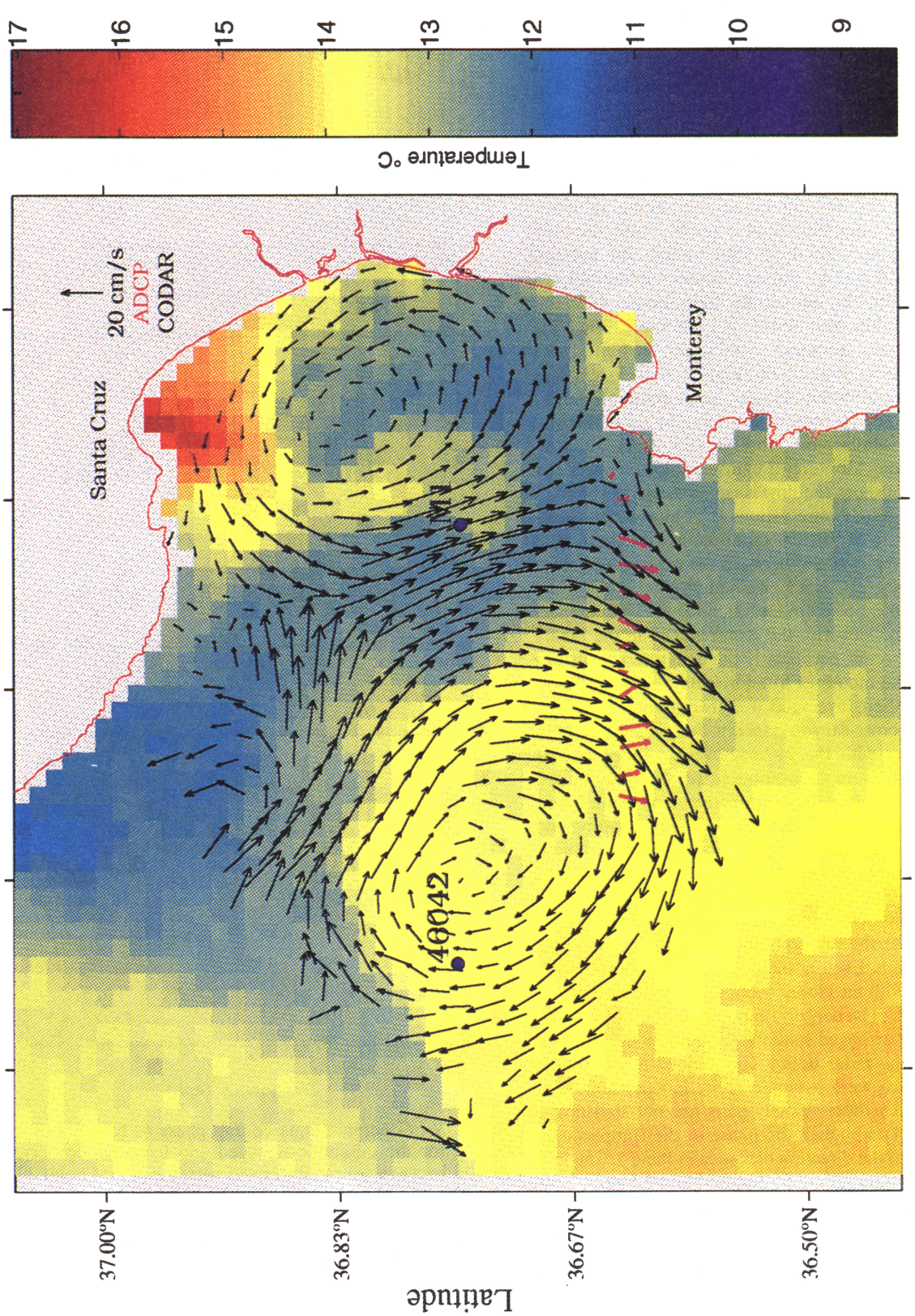

Plate 1. Average radar-derived vectors for the period 0900 UT on August 6 to 0700 UT on August 7, 1994 (black arrows), and average VM-ADCP vectors for the period 1016 UT on August 6 to 0524 UT on August 7, 1994 (magenta arrows), shown with uncorrected AVHRR channel 4 surface temperatures from 0300 UT on August 6, 1994.

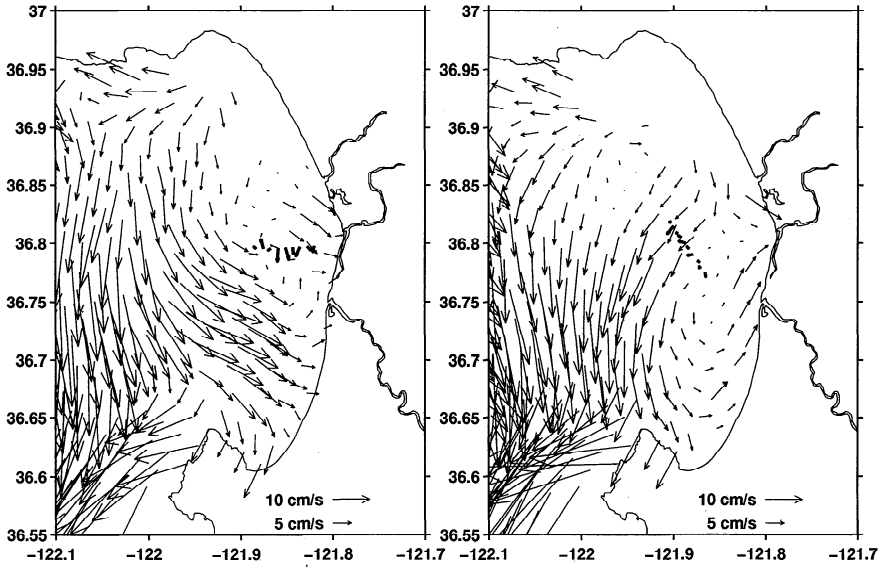

Figure 8. Average radar-derived vectors (thin arrows) and VM-ADCP vectors (heavy arrows) for the periods (left) 1700 UT on October 29 to 1900 UT on October 30, 1994, and (right) 1900 UT on October 30 to 2100 UT on October 31, 1994.

a complete set of maps showing both radar-derived and drifter-derived currents. Here we summarize the results.

Maps showing both drifter-derived and radar-derived vectors are presented in Figure 9. Clearly, current patterns observed in drifter trajectories are reproduced in the HF radar data. These examples represent some of the best comparisons from the two experiments. Histograms of the velocity difference between drifter-derived and radar-derived currents are shown in Figure 10. The upper panels show the comparisons for the combined data set from the 1992 and 1994 drifter deployments. A total of 160 HF radar-drifter velocity pairs are included in these statistics. The rms velocity differences are 16.2 cm s^{-1} and 13.6 cm s^{-1} for the u and v components, respectively. The rms speed difference is 12.8 cm s^{-1} and the rms direction difference is 63.7° (Table 1). The average comparisons alone are much greater than the 4 cm s^{-1} resolution of the radar technique. However, observations are clearly skewed toward agreement: 50% of the velocity component differences are under 7 cm s^{-1}. Relatively few observations with very large disagreement heavily influence the average statistics. Results for the subset based on CODE-type drifters only, which includes 39 velocity pairs, show slightly better comparisons: rms differences are 15.8 cm s^{-1} and 11.9 cm s^{-1} for the u and v components, respectively, and 50% of the component differences are under 5 cm s^{-1}. The rms speed difference for this subset is 12.5 cm s^{-1} and the rms direction difference is 57.8°.

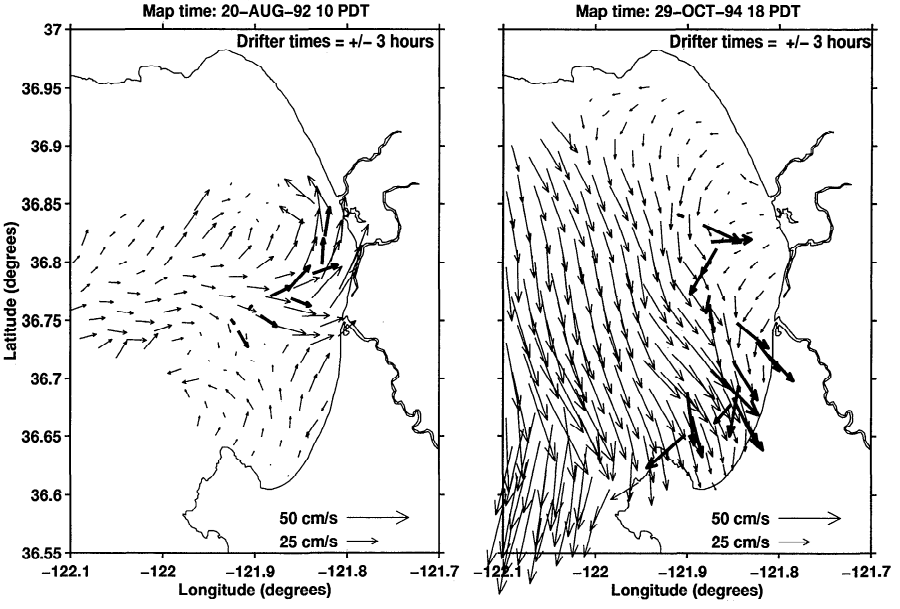

Figure 9. Radar-derived (thin arrows) and drifter-derived (heavy arrows) vectors for (left) 1700 UT on August 20, 1992, and (right) 0100 UT on October 30, 1994. Drifter vectors derive from available velocity estimates centered within 3 hours of times of the radar maps.

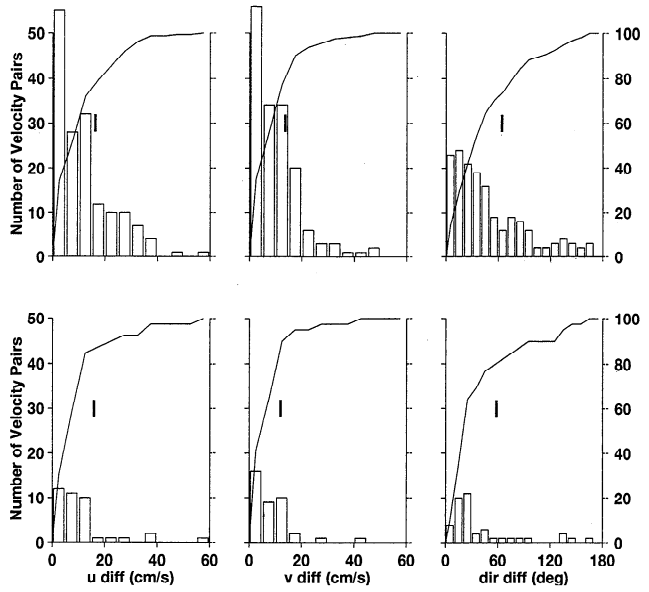

Figure 10. Distribution of velocity component and direction differences between radar- and drifter-derived currents from the drifter verification experiments in August 1992 and October 1994. Statistics for (top) the combined data set and (bottom) the CODE-type drifters from 1994 only are shown. Vertical-bar symbols denote rms differences, and solid lines show the cumulative percentages.

4. Low-Frequency Surface Current Patterns

In this section we present low-frequency surface current patterns around Monterey Bay. As shown in the last section the radar-derived current fluctuations compare favorably with in situ measurements for subtidal frequencies. Here we exploit that fact to present a unique, two-dimensional view of surface currents based on HF radar data averaged over, at least, 1 month. For the 2-hourly observations this represents the result of combining at least 336 current maps, depending on the month.

The statistical reliability of these averaged currents can be characterized by the 95% standard error of the mean, which is computed as $u_{\mathrm{err}} = (2\sqrt{\sigma_u^2})/(\sqrt{N^*})$ for the u velocity component. This statistical error depends on the standard deviation σ_u and the number of independent observations of current, N^*. A similar formula holds for v velocity observations. N^* is computed using the independence timescales of 36 hours and 72 hours for u and v motions, respectively, described in the last section. For our 2-hourly data the number of independent observations is therefore $N^* = N/18$ or $N^* = N/36$, where N is the number of observations used in the average for a particular radar bin. N is not constant across the observation area as shown in Figure 2. Hence the standard error gives some measure of data coverage as well as data variance within the averaging period. In most cases the standard errors of the averaged currents we present are comparable to or larger than the mean currents, which indicate that time series longer than 1 month are needed to unequivocally separate the mean currents from the combination of random errors in the radar-derived currents plus true ocean variability. The largest signals in the radar-derived currents at all locations in this study derive from tidal-period motions, including sea breeze–driven currents. These motions are the subject of ongoing investigations, but for the low-frequency motions in this study they are responsible for large variances and standard errors. This would be true even in the presence of no instrument error, which is not the case here. It should also be remembered that bias errors in the radar observations or algorithms are not exposed using this statistical measure.

4.1. August-December Mean Currents

Mean radar-derived surface currents during the entire 5-month period from August through December 1994 are presented in Figure 11 at grid points with observations at least 50% of the time. (The percent temporal coverage over this period was presented in Figure 2.) Standard errors of these mean currents are presented in Figure 11 as vectors whose lengths can be used to gauge the statistical reliability of the mean vectors. The typical 60° angle of the error vectors indicates that v_{err} is larger than u_{err}, which is due to the longer v independence timescale. Despite uncertainties about the error sources and high standard errors the average current patterns we observe in the radar data are both physically realistic and consistent with historical observations. Persistent equatorward flow is seen just offshore of Monterey Bay with mean speeds of about 20 cm s^{-1}. Within the bay the 5-month averaged current field exhibits a single circulation cell with cyclonic rotation. The center of this cell has near-zero mean currents and is located about 15 km northwest of Moss Landing. The predominantly northward mean flow along the coast has speeds of 5–7 cm s^{-1}. There is evidence in this 5-month mean pattern of a

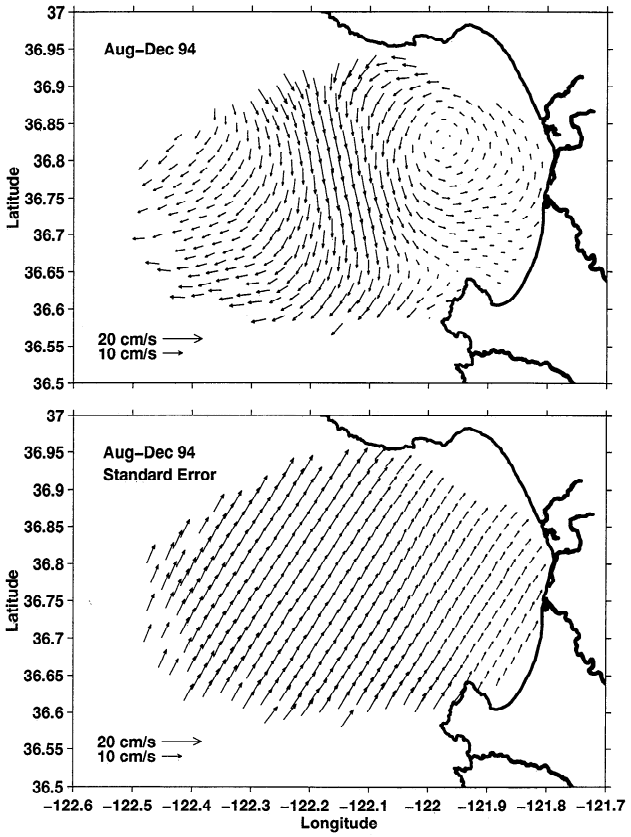

Figure 11. (top) Average radar-derived current vectors and (bottom) standard error vectors for the period August–December 1994 for grid points with at least 50% temporal coverage. Standard errors assume independence timescales of 36 hours and 73 hours for u and v motions, respectively.

stagnation point along the coast between Moss Landing and Monterey. The mean currents in the bight between this stagnation point and the Monterey Peninsula are weak (<3 cm s^{-1}). There are suggestions in the shorter-period observations that a smaller anticyclonic circulation pattern occurs at times in this area. Point Pinos at the northern tip of the Monterey Peninsula is, in this data, a transition site where low-pass-filtered currents are observed to flow along the coast in both directions at different times. This is more clearly seen in the monthly averages.

4.2. Monthly Averaged Currents

In spite of the fact that a month is not long enough to produce highly statistically significant means (standard errors are 100–200% of the means), the monthly averaged currents in this study show robust patterns that transition smoothly from August through December. We can show that the 5-month averaged patterns described above are dominated by strong and persistent currents in the August and September data. October and November data, on the other hand, exhibit stronger week-to-week variability and December monthly averaged currents, though also based on strongly variable currents, show regions of mean northward flow in the outer part of Monterey Bay, which is opposite to the common summer situation.

The particularly strong "summer-type" circulation seen in August 1994 is shown in Figure 12. The patterns are similar to those described for the 5-month averaged currents, although the speeds are consistently larger. The southward currents in the outer portion of the study area exceed 25 cm s^{-1} in the monthly mean, and the along-coast northward flow within Monterey Bay is 10–20 cm s^{-1}. There is no evidence of the weaker anticyclonic circulation pattern in the southern part of the bay in the August mean currents. Average currents east of Point Pinos are clearly southeastward, consistent with a single cyclonic circulation pattern. Averaged currents for September 1994 (Figure 13) are similar to the August currents but noticeably weaker throughout the study area.

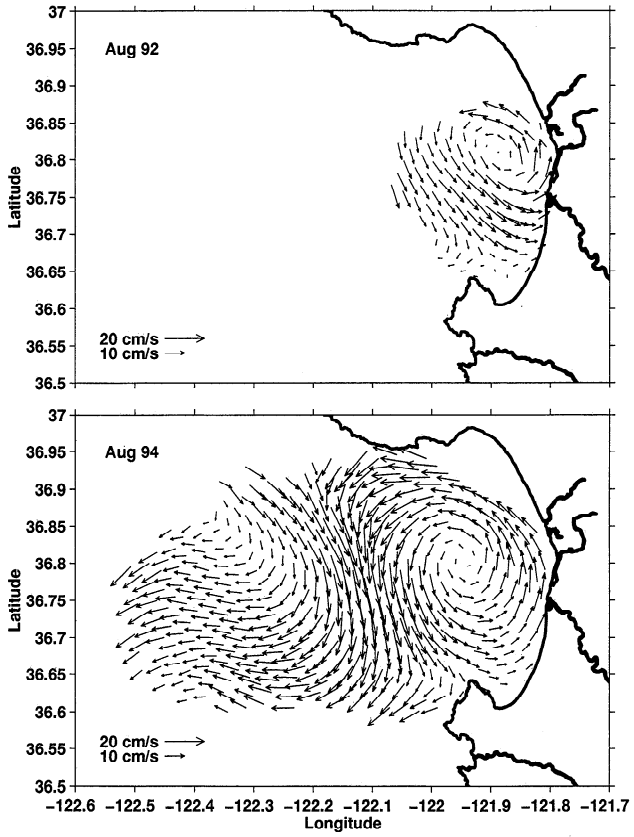

Figure 12. Average radar-derived current vectors for (top) August 1992 and (bottom) August 1994 for grid points with at least 50% temporal coverage.

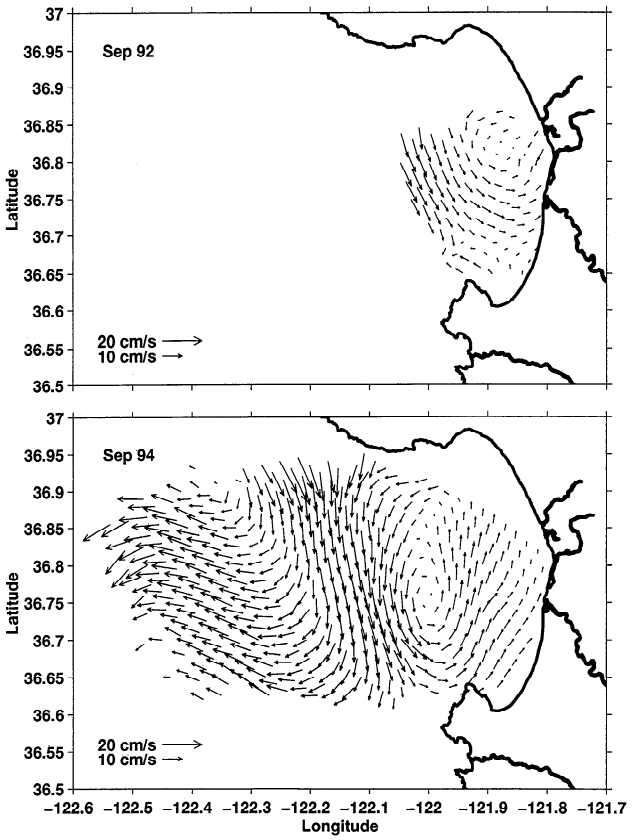

Figure 13. Average radar-derived current vectors for (top) September 1992 and (bottom) September 1994 for grid points with at least 50% temporal coverage.

The monthly averaged HF radar data from October 1994 (Figure 14) and November 1994 (not shown) illustrate the current patterns during the fall transition. The clear cyclonic circulation pattern found within Monterey Bay during summer is absent. Offshore of the bay, currents are still consistently southward with mean speeds of 10–15 cm s^{-1}. November results are similar to those from October except that the mean southward currents offshore are even weaker (under 10 cm s^{-1}). The average radar-derived currents for December 1994 are also shown in Figure 14. The mean flow across the mouth of Monterey Bay is poleward during this month. Week-to-week maps of radar-derived currents show that this pattern derives from episodes of northward flow in this area, which persist for several days at a time. These events can be seen in the time series shown in Figure 4. Although northward flow is evident beginning in August, the strongest and most persistent northward currents at the M1 location occur in November and December.

Radar-derived current fields during April–September 1992 derived from the original, two-site CODAR network show circulation patterns similar to those observed during the sum-

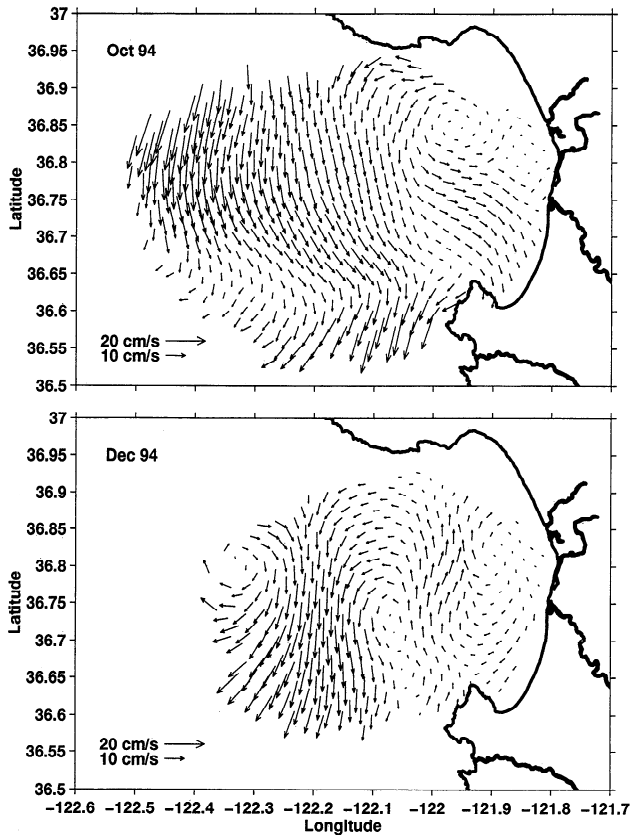

Figure 14. Average radar-derived current vectors for (top) October 1994 and (bottom) December 1994 for grid points with at least 50% temporal coverage.

mer of 1994. The spatial coverage from that earlier network was much less than that of the present three-site network, which is why we have given more attention to the 1994 data in this study. Monthly averaged currents from April, May, August, and September 1992 exhibit summer-type circulation [*Neal*, 1992; *Foster*, 1993]. Data are not available for June and July of that year, but, presumably, the summer-type pattern existed for, at least, the April–September period in 1992. The mean radar-derived current fields for August 1992 and September 1992 are shown in Figures 12 and 13, respectively, together with their counterparts from 1994. Although the instruments and coverages from the 2 years are different, similar cyclonic circulation patterns are seen during both summers, including stronger currents in August than in September.

The general view of surface current patterns around Monterey Bay from HF radar data for 1992 and 1994 is that of summer-type circulation from April through September with a transition period in October–November. Summer-type circulation is defined by a dominant cyclonic circulation cell within Monterey Bay and southward flow offshore of the bay. Frequent northward flow in the outer part of the bay occurs during the fall transition period and can be manifest as monthly averaged northward flows by December, which is consistent with historical views of wintertime currents off the coast of Central California [*Hickey*, 1979].

5. Discussion and Summary

The HF radar-derived velocity fields during late summer 1992 and 1994 reveal a band of equatorward flow across the mouth of Monterey Bay with cyclonic circulation inside the bay and anticyclonic circulation offshore. This late summer flow pattern is very similar to our prior understanding of the April–July flow patterns in the Monterey Bay area based on AVHRR imagery, drifter measurements, CTD data, and both vessel-mounted and moored ADCP observations [*Rosenfeld et al.*, 1994a, 1995]. Furthermore, our detailed comparisons of low-pass-filtered moored current measurements and HF radar-derived currents in the outer part of the bay show high correlations (~0.79) based on time series from August to December 1994 (Table 1). Velocity differences between radar-derived and ADCP currents are highly correlated with wind stress. This correlation is, at least, partially explained by expected current shear between 1 m and 9 m depths and by wave-induced Stokes drift, which is present in the radar-derived currents, but not in the ADCP currents. Interestingly, the radar-ADCP velocity differences are not highly correlated with near-surface temperature stratification at the mooring site. Therefore momentum trapping in a thin, buoyant layer at the surface is not the primary reason for the differences observed. The onshore-offshore (u) velocity differences do exhibit a weakly significant and negative correlation with temperature stratification (Table 1). This can be interpreted to mean that near-surface stratification was typically largest (smallest) during periods of westward (eastward) flow.

As discussed by *Rosenfeld et al.* [1994a], it is felt that equatorward flow appearing in a band across the mouth of Monterey Bay is associated with the advection of wind-driven coastal upwelled water from the Año Nuevo upwelling center. Radar-derived currents overlain on the AVHRR image of August 6, 1994 (Plate 1), also support this hypothesis. Offshore of this region of equatorward flow, meanders of the California Current with anticyclonic circulation have often been reported [*Breaker and Broenkow*, 1994; Ramp et al., submitted manuscript, 1996], and such a situation is also visible in the AVHRR and HF radar data in Plate 1. The cyclonic circulation within Monterey Bay revealed by the HF radar network is consistent with the circulation observed by drifters [*Moomy*, 1973] and the westward flow in the northern bight of Monterey Bay measured by current meters [*Brown and Caldwell Engineers*, 1979] and hypothesized by *Graham et al.* [1992] based on hydrographic data.

Although there are less historical data with which to compare the fall currents, the presence of increased variability on weekly timescales and increased occurrence of poleward flow at the outer portions of Monterey Bay is consistent with our understanding of the fall and winter conditions along the central California coast. This increased variability late in the year is related to increased variability in the low-frequency winds. The narrow band of poleward flow observed in the December 1994 mean radar-derived current map may be a manifestation of the Davidson Current, sometimes thought to be a shoaling of the California Undercurrent. A narrow band of poleward geostrophic flow was observed nearshore off Point Sur in November 1988 and 1989 [*Tisch et al.*, 1992]. Data from brief drifter deployments in the 1950s and 1970s are also consistent with weak or slightly poleward surface flows in the outer parts of Monterey Bay during the fall and winter [*Reid and Schwartzlose*, 1962; *Griggs*, 1974].

The time series analyses conducted with HF radar data show significant coherence with winds for both low-frequency motions and energetic tidal frequencies, while, at the same location, the coherences between SC-ADCP currents at 9 m and

winds are not significant for subtidal frequencies. The phase relationship between wind and radar-derived currents at low frequencies is close to the theoretical 45° predicted by classical, steady state Ekman theory. At higher frequencies, *Neal* [1992] and *Foster* [1993] both show strong diurnal signals in the CODAR data from 1992, which were related to sea breeze wind forcing. *Petruncio* [1993] shows radar-derived semidiurnal tidal ellipses from September 1992 that vary spatially with the bottom topography in that amplitudes are largest over the head of the Monterey Submarine Canyon, just a few kilometers from Moss Landing, and ellipse orientations align with the shelf break along the sides of the canyon. SC-ADCP data from 17 m during September 1992 show semidiurnal fluctuations that are similar in amplitude to those in the CODAR data from 1 m, while showing diurnal fluctuations that are an order of magnitude weaker than those at 1 m. This reinforces the idea that the ocean response to wind forcing at high frequencies is largely confined to the upper few meters. Future HF radar observations may be able to expose even more details of the turbulent momentum transfer very near the surface, especially if they are combined with better moored techniques for measuring near the surface, such as high-frequency upward looking ADCPs.

In this study we have used the HF radar velocity data as processed by the manufacturer. Our goal was to evaluate the usefulness of this remote sensing technique and to suggest ways to improve it in the future. On the basis of the data presented here we cannot report an expected accuracy of individual CODAR vectors, such as 95% of the time the value will be within $\pm x$ cm s^{-1} of the true value. We have shown that the statistical standard error of the mean is similar to the mean for months-long averages, although this does not address potential instrument biases. Quantitative comparison of filtered radar and SC-ADCP currents yielded rms speed differences of 6–11 cm s^{-1} and rms direction differences of about 51°; comparison of unfiltered radar and drifter-derived currents yielded rms speed differences of 10–17 cm s^{-1} and rms direction differences of about 64° (Table 1). All differences were heavily skewed toward better agreement, however, with most of the differences less than these rms values. This can be seen in the histograms of radar-drifter velocity differences in Figure 10 and in the difference between rms and median values in Table 1. If, for the sake of argument, we assume error-free ADCP and drifter measurements and attribute observed differences to radar error, then these results are consistent with a remote sensing radar measurement that is accurate 50% of the time to within 7 cm s^{-1} and subject to infrequent but very large errors at other times. There is some evidence that these large errors are random because low-pass filtering improves the radar versus in situ comparisons. However, sources of bias to the radar measurements, such as distorted antenna patterns or inhomogeneity of the surface wave field, should be investigated in future studies.

Of course, the "ground truth" data used here are not error free, and real differences in the timescales and space scales of the different measurements will further limit their agreement. In particular, the drifter velocity estimates used here are, themselves, subject to large errors due to position errors and windage on the instruments. The best agreements between radar and drifter-derived velocities in this study were obtained for CODE-type drogued drifters positioned by the Argos system [*Paduan et al.*, 1996]. Future efforts to validate HF radar-derived currents with drifters could be optimized by using similar CODE-type drifters equipped with GPS receivers and packet radio transmitters for local telemetry of data to shore.

We feel that the results presented here show that CODAR-type HF radar observations are promising enough to warrant further use and stepped-up efforts to quantify errors and improve processing algorithms. There is a huge potential for these instruments, and HF radars in general, to provide direct observations of coastal surface currents for both long-term studies of coastal dynamics and real time applications, such as hazardous spill tracking, search and rescue operations, and marine forecasts. These instruments require better error detection and quantification than are presently available, particularly for real time uses. Steps that may be taken immediately by users of HF radar data include the following: incorporate information about mapping errors involved in the transformation from radial component observations to vector velocity maps [*Prandle*, 1991], incorporate checks in the vector processing to exploit the fact that two systems should measure the same radial velocity component from opposite directions along the baselines, exploit the overdetermination of surface currents in regions with three-site coverage to evaluate uncertainty in the vector computations, and, possibly, identify periods when individual radar sites are malfunctioning.

Perhaps the most important source of error to investigate relative to HF radars is the impact of antenna distortion on the radial velocity estimates. In the case of direction-finding systems (e.g., CODAR and SeaSonde), distortion of the expected antenna patterns will result in error in the angular location of radial data. In the case of phased-array systems (e.g., OSCR), distortion of the patterns will result in error in the magnitude of radial data. In both cases the resulting maps of vector velocities will be in error, particularly under oceanographic conditions of strong currents or strong horizontal current shear. Direct field calibration of antenna patterns must be conducted, and their impact on processing schemes must be evaluated, for every deployment of an HF radar system. Direction-finding systems suffer from the added problem of low radial data coverage if the range of ocean current speeds is small. This is because radial current values within 4 cm s^{-1} bins can be assigned to, at most, two angular directions within a given range cell [*Lipa and Barrick*, 1983]. The implications of this restriction under various current, wind, and sea state conditions must be investigated.

Acknowledgments. Members of the Monterey Bay HF Radar Consortium helped to install and operate the radar systems used in this study. The Consortium includes participants from NOAA, the Naval Postgraduate School, Stanford University, MBARI, the University of California at Santa Cruz, and the U.S. Coast Guard. Meteorological observations from the MBARI mooring were supplied by Francisco Chavez, surface drifters were donated by Walter Johnson and James Price of the Minerals Management Service, and collection of VM-ADCP data was supported by the Oceanographer of the Navy and by NSF grant OCE-9116408 to L. Rosenfeld. Michael Cook, Gerry Hatcher, and Todd Anderson helped with many of the computations and figures, Thomas Kinder made helpful comments on the manuscript, and Laurence Breaker provided programs for computing vector correlations. The authors were supported by research funds of the Naval Postgraduate School and MBARI and by the Office of Naval Research under contract N0001495WR30022 within the Naval Ocean Modeling and Prediction Program.

References

Barrick, D. E., The role of the gravity-wave dispersion relation in H.F. radar measurements of the sea surface, *IEEE J. Oceanic Eng., OE 11*, 286–292, 1986.

Barrick, D. E., M. W. Evans, and B. L. Weber, Ocean surface currents mapped by radar, *Science, 198*, 138–144, 1977.

Bevington, P. R., *Data Reduction and Error Analysis for the Physical Sciences*, 336 pp., McGraw-Hill, New York, 1969.

Bolin, R. L., and D. P. Abbot, Studies on the marine climate and phytoplankton of the central coastal area of California, 1954–1960, *Calif. Coop. Fish. Invest., 9*, 23–45, 1963.

Breaker, L. C., and W. W. Broenkow, The circulation of Monterey Bay and related processes, *Oceanogr. Mar. Biol., 32*, 1–64, 1994.

Breaker, L. C., W. H. Gemmill, and D. S. Crosby, The application of a technique for vector correlation to problems in meteorology and oceanography, *J. Appl. Meteorol., 33*, 1354–1365, 1994.

Brown and Caldwell Engineers, Monterey Bay environmental sensitivity study, prepared for the Regional Water Quality Control Board Central Coastal Region, Brown and Caldwell Engineers, Walnut Creek, Calif., 1979.

Chelton, D. B., Seasonal variability of alongshore geostrophic velocity off central California, *J. Geophys. Res., 89*, 3473–3486, 1984.

Chelton, D. B., R. L. Bernstein, A. Bratkovich, and P. M. Kosro, The Central California Coastal Circulation Study, *Eos Trans. AGU, 68*, 1, 12–13, 1987.

Crombie, D. D., Doppler spectrum of sea echo at 13.56 Mc/s, *Nature, 175*, 681–682, 1955.

Crosby, D. S., L. C. Breaker, and W. H. Gemmill, A proposed definition for vector correlation in geophysics: Theory and application, *J. Atmos. Oceanic Technol., 10*, 355–367, 1993.

Davis, R. E., Drifter observations of coastal surface currents during CODE: The methods and descriptive view, *J. Geophys. Res., 90*, 4741–4755, 1985.

Fernandez, D. M., High-frequency radar measurements of coastal ocean surface currents, Ph.D. dissertation, 191 pp., Stanford Univ. Stanford, Calif., 1993.

Foster, M. D., Evolution of diurnal surface winds and surface currents for Monterey Bay, M.S. thesis, 100 pp., Naval Postgrad. School, Monterey, Calif., 1993.

Gonella, J., A rotary-component method for analyzing meteorological and oceanographic vector time series, *Deep Sea Res., 19*, 833–846, 1972.

Graham, W. M., J. G. Field, and D. C. Potts, Persistent "upwelling shadows" and their influence on zooplankton distributions, *J. Mar. Biol., 112*, 561–570, 1992.

Griggs, G. B., Nearshore current patterns along the central California coast, *Estuarine Coastal Mar. Sci., 2*, 395–402, 1974.

Gurgel, K.-W., Shipborne measurements of surface current fields by HF radar, *Onde Électr., 74*, 54–59, 1994.

Ha, E. C., Remote sensing of ocean surface current and current shear by HF backscatter radar, *Tech. Rep. D415-1*, Stanford Elect. Lab., Stanford Univ., Stanford, Calif., 1979.

Hayes, S. P., System Users Guide, ATLAS moored wind and thermistor chain array, Pac. Mar. Environ. Lab., NOAA, Seattle, Wash. 1989.

Hickey, B. M., The California Current System—hypotheses and facts, *Prog. Oceanogr., 8*, 191–279, 1979.

Joyce, T. M., On in situ "calibration" of shipboard ADCPs, *J. Atmos. Oceanic Technol., 6*, 169–172, 1989.

Kundu, P. K., Ekman veering observed near the ocean bottom, *J. Phys. Oceanogr., 6*, 238–242, 1976.

LeBlond, P. H., and L. A. Mysak, *Waves in the Ocean*, 602 pp., Elsevier, New York, 1978.

Lipa, B. J., and D. E. Barrick, Least-squares method for the extraction of surface currents from CODAR crossed-loop data: Application at ARSLOE, *IEEE J. Oceanic Eng., OE 8*, 226–253, 1983.

Lynn, R. J., and J. J. Simpson, The California Current System: The seasonal variability of its physical characteristics, *J. Geophys. Res., 92*, 12,947–12,966, 1987.

Masson, D., A case study of wave-current interaction in a strong tidal current, *J. Phys. Oceanogr., 26*, 359–372, 1996.

McLeish, W., and G. A. Maul, CODAR in the Straits of Florida: Final report, *NOAA Tech. Rep. ERL 447-AOML 35*, 46 pp., 1991.

Mooers, C. N. K., A technique for the cross spectrum analysis of pairs of complex-valued time series, with emphasis on properties of polarized components and rotational invariants, *Deep Sea Res., 20*, 1129–1141, 1973.

Moomy, D. H., Temperature variations throughout Monterey Bay, September 1971–October 1972, M.S. thesis, 166 pp., Naval Postgrad. School, Monterey, Calif., 1973.

Neal, T. C., Analysis of Monterey Bay CODAR-derived surface currents, March to May 1992, M.S. thesis, 96 pp., Naval Postgrad. School, Monterey, Calif., 1992.

Nelson, C. S., Wind stress and wind stress curl over the California Current, *NOAA Rep. NMFS SSRF-714*, 87 pp., 1977.

Paduan, J. D., M. H. Pickett, and M. S. Cook, Comparison of surface currents from satellite-tracked drifting buoys and HF radar (CODAR) in Monterey Bay, *NOAA Rep. MBNMS 96-01*, 35 pp., 1996.

Petruncio, E. T., Characterization of tidal currents in Monterey Bay from remote and in-situ measurements, M.S. thesis, 113 pp., Naval Postgrad. School, Monterey, Calif., 1993.

Prandle, D., A new view of near-shore dynamics based on observations from HF radar, *Prog. Oceanogr., 27*, 403–438, 1991.

Prandle, D., and D. K. Ryder, Measurement of surface currents in Liverpool Bay by high-frequency radar, *Nature, 315*, 128–131, 1985.

Prandle, D., and D. K. Ryder, Comparison of observed (HF Radar) and modeled near-shore velocities, *Cont. Shelf Res., 9*, 941–963, 1989.

Prandle, D., S. G. Loch, and R. Player, Tidal flow through the Straits of Dover, *J. Phys. Oceanogr., 23*, 23–37, 1993.

RD Instruments, Acoustic Doppler Current Profilers, Principles of operation: A practical primer, technical report, 36 pp., San Diego, Calif., 1989.

Reed, M., C. Turner, A. Odulo, T. Isaji, S. E. Sørstrøm, and J. P. Mathisen, Field evaluation of satellite-tracked surface drifting buoys in simulating the movement of spilled oil in the marine environment, *Rep. MMS 90-0050*, 37 pp., Miner. Manage. Serv., U.S. Dep. of the Int., Washington, D. C., 1990.

Reid, J. L., and R. A. Schwartzlose, Direct measurements of the Davidson Current off central California, *J. Geophys. Res., 67*, 2491–2497, 1962.

Rosenfeld, L. K., F. B. Schwing, N. Garfield, and D. E. Tracy, Bifurcated flow from an upwelling center: A cold water source for Monterey Bay, *Cont. Shelf Res., 14*, 931–964, 1994a.

Rosenfeld, L. K., R. E. Schramm, J. B. Paduan, G. A. Hatcher, and T. Anderson, Hydrographic data collected in Monterey Bay during 1 September 1988 to 16 December, 1992, *Tech. Rep. 94-15*, 549 pp., Monterey Bay Aquarium Res. Inst., Moss Landing, Calif., 1994b.

Rosenfeld, L., T. Anderson, G. Hatcher, J. Roughgarden, and Y. Shkedy, Upwelling fronts and barnacle recruitment in Central California, *Tech. Rep. 95-19*, 102 pp., Monterey Bay Aquarium Res. Inst., Moss Landing, Calif., 1995.

Shay, L. K., H. C. Graber, D. B. Ross, and R. D. Chapman, Mesoscale ocean surface current structure detected by high-frequency radar, *J. Atmos. Oceanic Technol., 12*, 881–900, 1995.

Shkedy, Y., D. Fernandez, C. Teague, J. Vesecky, and J. Roughgarden, Detecting upwelling along the central coast of California during an El-Niño year using HF radar, *Cont. Shelf Res., 15*, 803–814, 1995.

Skogsberg, T., Hydrography of Monterey Bay, California. Thermal conditions, 1929–1933, *Trans. Am. Philos. Soc., 29*, 152 pp., 1936.

Skop, R. A., D. B. Ross, N. J. Peters, and L. Chamberlain, Measurements of coastal currents using a ship based VHF radar system, *RSMAS Tech. Rep. 94-001*, 25 pp., Univ. Miami, Miami, Fla., 1994.

Stewart, R. H., and J. W. Joy, HF radar measurement of surface current, *Deep Sea Res., 21*, 1039–1049, 1974.

Strub, P. T., J. S. Allen, A. Huyer, R. L. Smith, and R. C. Beardsley, Seasonal cycles of currents, temperatures, winds, and sea level over the northeast Pacific continental shelf: 35°N to 48°N, *J. Geophys. Res., 92*, 1507–1526, 1987.

Teague, C. C., Multifrequency HF radar observations of currents and current shears, *IEEE J. Oceanic Eng., OE 11*, 258–269, 1986.

Tisch, T. D., S. R. Ramp, and C. A. Collins, Observations of the geostrophic current and water mass characteristics off Point Sur, California, from May 1988 through November 1989, *J. Geophys. Res., 97*, 12,535–12,555, 1992.

Wickham, J. B., Observations of the California Countercurrent, *J. Mar. Res., 33*, 325–340, 1975.

Wyllie, J. G., *Geostrophic Flow of the California Current at the Surface and at 200 m, California Cooperative Oceanic Fisheries Investigations Atlas 4*, 13 pp. and 288 charts, Calif. Coop. Oceanic Fish. Invest., La Jolla, 1966.

J. D. Paduan and L. K. Rosenfeld, Department of Oceanography, Naval Postgraduate School, Monterey, CA 93943. (e-mail: paduan@oc.nps.navy.mil)

(Received August 10, 1995; revised May 8, 1996;
accepted May 22, 1996.)